

Supplementary Information File

Effect of Salt Variability on the Low-temperature Metal-Catalyzed Graphitization of PAN/DMSO Solutions for the Synthesizing Nanostructured Graphitic Carbon

Taewoo Kim ^{a, b}, Byoung-Sukh Kim^{b, c}, Tae Hoon Ko ^{a, b*}, Hak Yong Kim ^{a, b*}

^aDepartment of Nano Convergence Engineering, Jeonbuk National University, Jeonju-561756, Republic of Korea

^b Department of Organic Materials and Textile Engineering, Jeonbuk National University, Jeonju-561756, Republic of Korea

^c Carbon Composites Convergence Materials Engineering, Jeonbuk National University, Jeonju-561756, Republic of Korea

1. Experimental Section

1.1 Materials

Acrylonitrile ($\geq 99.0\%$), Itaconic acid ($\geq 99.0\%$), 1-Dodecanethiol ($\geq 98.5\%$), 2,2-Azobisisobutyronitrile (KOH, $\geq 98.0\%$), and DMSO ($\geq 99.0\%$) were obtained from Samchun, Republic of Korea. Lithium nitrate ($\text{LiNO}_3 \geq 99.0\%$), Calcium nitrate ($\text{Ca}(\text{NO}_3)_2 \geq 99.0\%$), and Nickel nitrate ($\text{Ni}(\text{NO}_3)_2 \geq 99.0\%$) are purchased from Sigma-Aldrich. All the chemical compounds were analytical grade and used without further purification.

2. Materials characterizations

The as-prepared materials' surface morphology, microstructural analysis, and elemental analysis of the fabricated samples were described using field emission scanning electron microscopy (FE-SEM, SUPRA40VP, Carl Zeiss, Germany) with an instrument equipped with energy-dispersive X-ray spectroscopy (EDXS) and transmission electron microscopy (TEM, JEM-2100 plus, JEOL Ltd., Japan). The phase, as well as the structure of all the samples, were studied with X-ray diffraction (XRD, Rigaku Corporation, Japan, CuK α radiation, wavelength $\lambda=0.154$ nm) in the 2θ range from 5-80° at a scan rate of 2° min⁻¹. The graphitization of all prepared samples was analyzed by Raman spectroscopy at room temperature using a Raman spectrometer (RAMANtouch) from Nanophoton, with an argon ion laser source at an excitation wavelength of 523 nm, conducted at the Gunsan National University Center for Research Facilities. FE-SEM, EDX, TEM, and XRD analyses were performed at the Center for University-wide Research Foundation (CURF), Jeonbuk National University, Jeonju, South Korea.



Figure S1: Photographic image PANs solution with different metal salt (catalyst) at

various wt%.

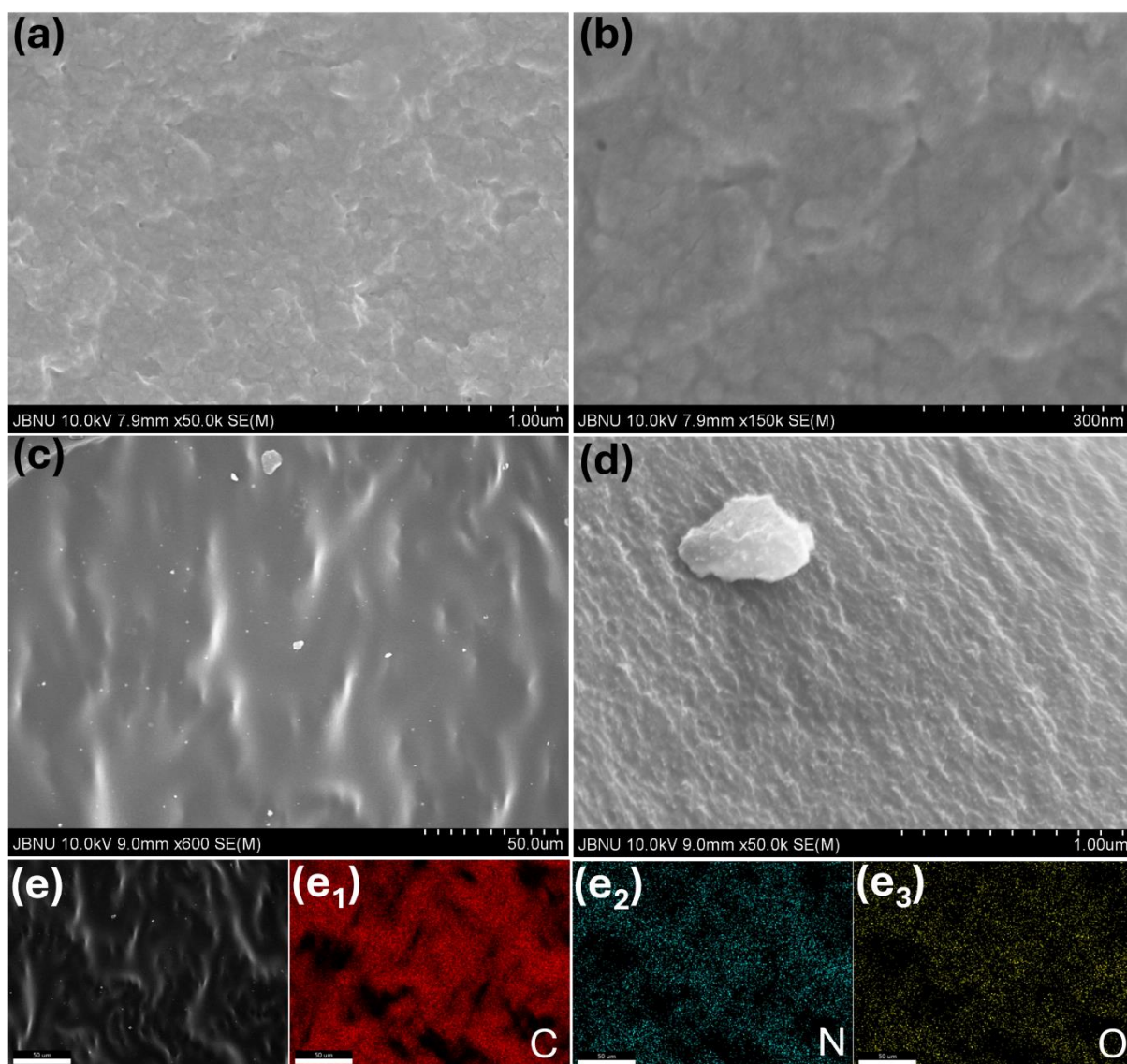


Figure S2: Fe-SEM image: (a, and b) PANs after the drying process, (c, and d) graphitized carbon (GC) of pure PANs after carbonization, and (e, e₁, e₂, and e₃) its elemental mapping.

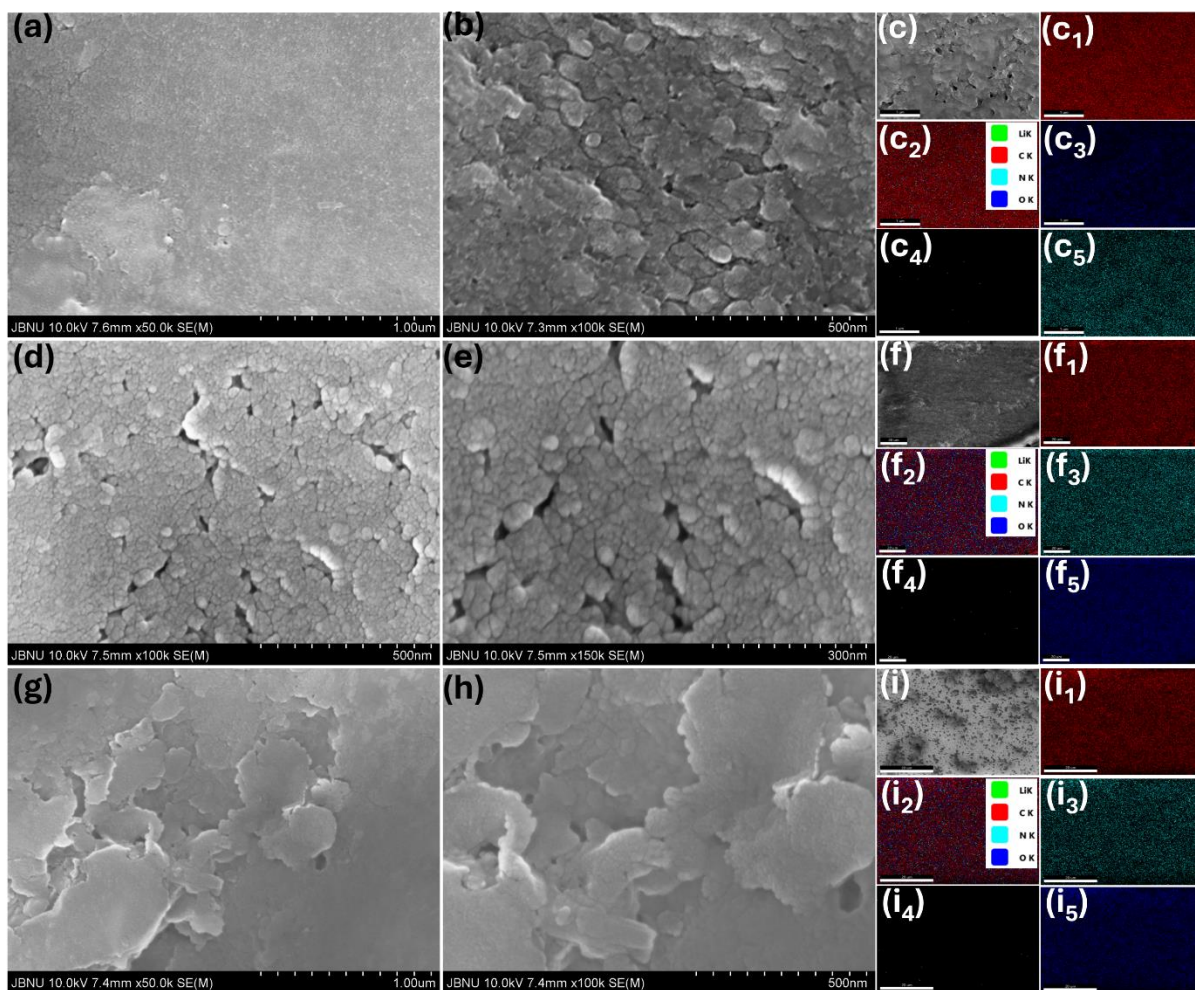


Figure S3: Morphological characterizations: (a, and b) FE-SEM images and (c, c₁, c₂, c₃, c₄, and c₅) elemental mapping of Li-PANs-5, (d, and e) FE-SEM images and (f, f₁, f₂, f₃, f₄, and f₅) elemental mapping of Li-PANs-10, (g, and h) FE-SEM images and (i, i₁, i₂, i₃, i₄, and i₅) elemental mapping of Li-PANs-15 after drying process.

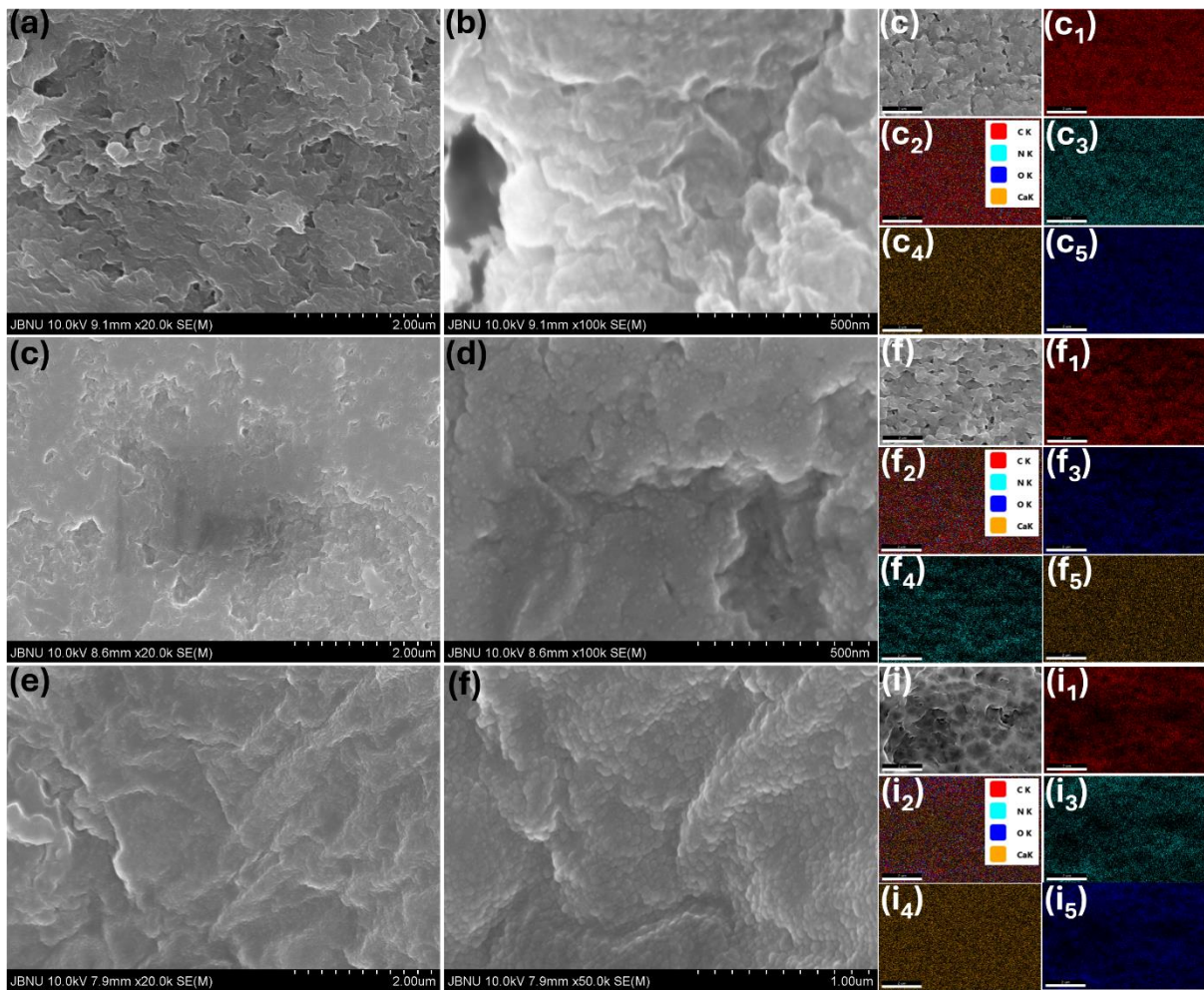


Figure S4: Morphological characterizations: (a, and b) FE-SEM images and (c, c₁, c₂, c₃, c₄, and c₅) elemental mapping of Ca-PANs-5, (d, and e) FE-SEM images and (f, f₁, f₂, f₃, f₄, and f₅) elemental mapping of Ca -PANs-10, (g, and h) FE-SEM images and (i, i₁, i₂, i₃, i₄, and i₅) elemental mapping of Ca -PANs-15 after drying process.

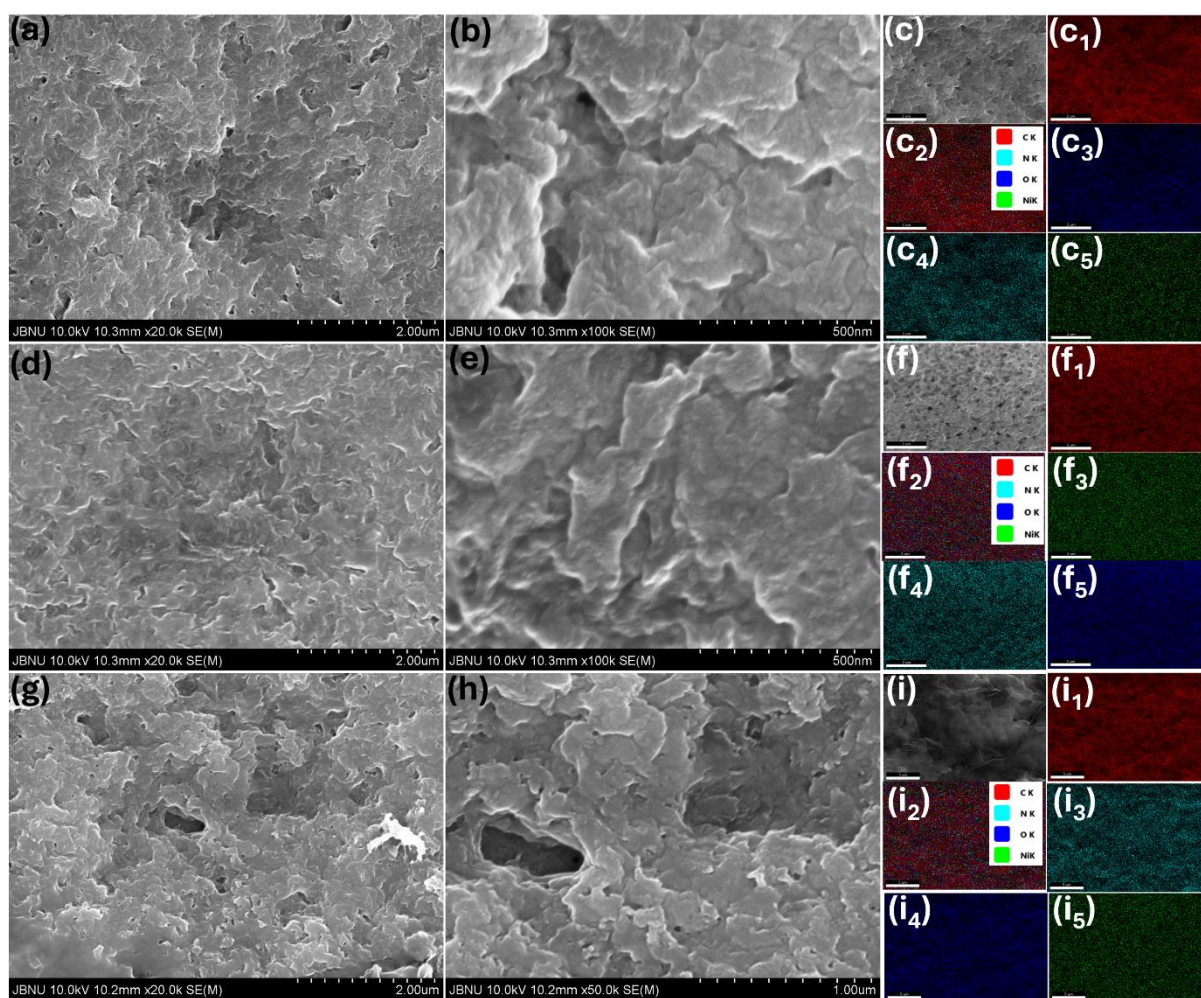


Figure S5: Morphological characterizations: (a, and b) FE-SEM images and (c, c₁, c₂, c₃, c₄, and c₅) elemental mapping of Ni-PANs-5, (d, and e) FE-SEM images and (f, f₁, f₂, f₃, f₄, and f₅) elemental mapping of Ni -PANs-10, (g, and h) FE-SEM images and (i, i₁, i₂, i₃, i₄, and i₅) elemental mapping of Ni -PANs-15 after drying process.

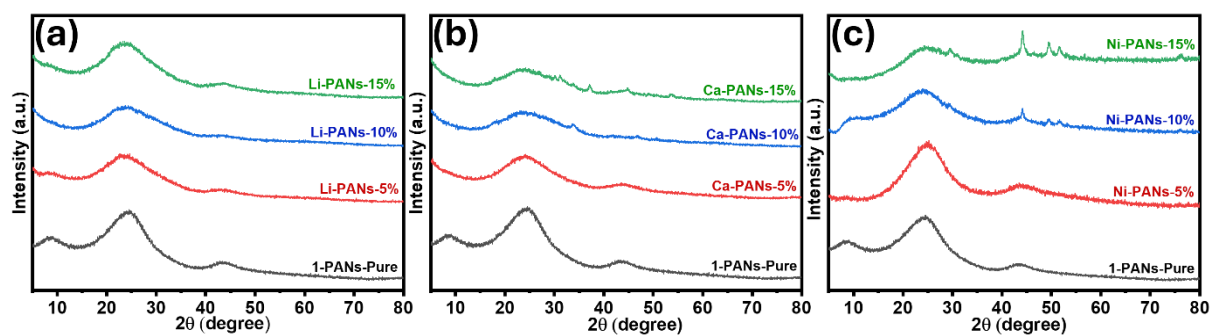


Figure S6: XRD analysis: (a) XRD pattern of Li-PANs-5, Li -PANs-10, and Li -PANs-15 (b) XRD pattern of Ca-PANs-5, Ca -PANs-10, and Ca-PANs-15, and (c) XRD pattern of Ni-PANs-5, Ni -PANs-10, and Ni -PANs-15 after drying process.

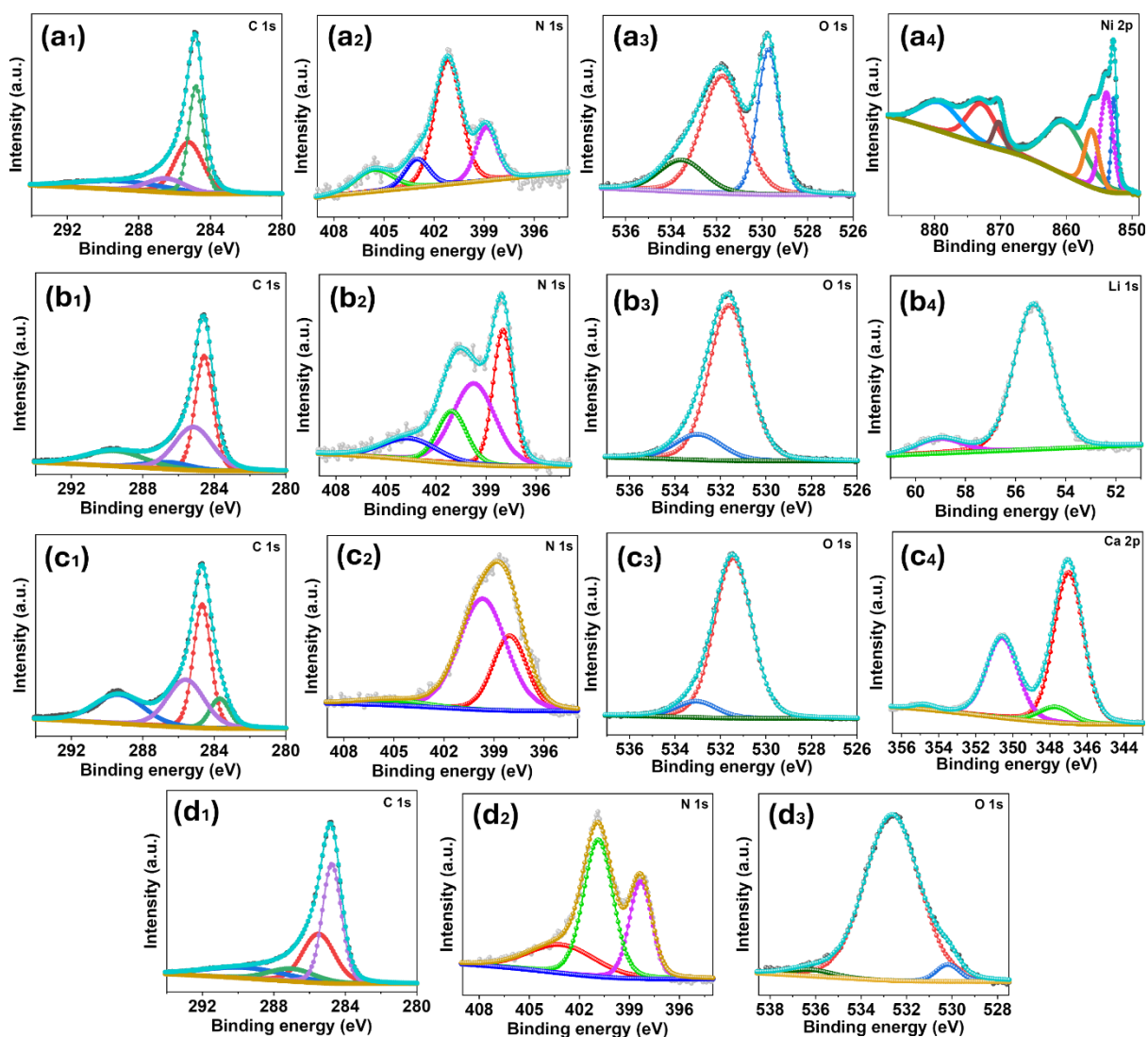


Figure S7: Deconvoluted XPS survey spectra of (a₁, a₂, a₃, and a₄) C1s, N1s, O1s, and Ni2p respectively of Ni-GC-15, (b₁, b₂, b₃, and b₄) C1s, N1s, O1s, and Li1s respectively of Li-GC-10, (c₁, c₂, c₃, and c₄) C1s, N1s, O1s, and Ca2p respectively of Ca-GC-5, (d₁, d₂, and d₃) C1s, N1s, and O1s respectively of Pristine GC.

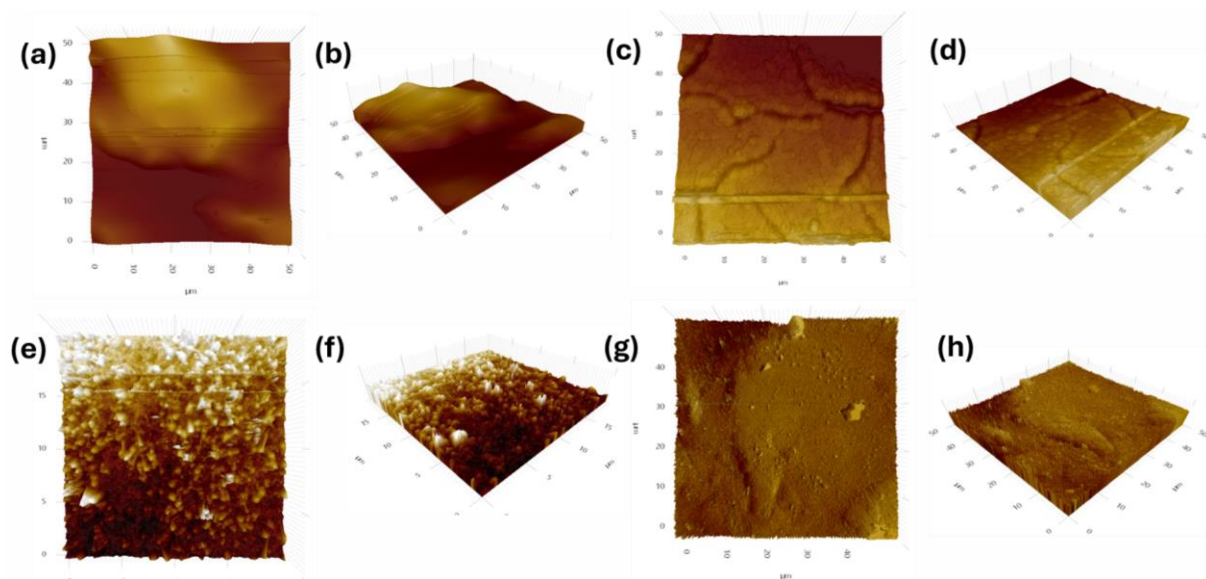


Figure S8: Top and tilted view AFM images of (a and b) Pristine GC, (c and d) Ca-GC-5, (e and f) Li-GC-10, and (g and h) Ni-GC-15.

Table S1: I_D/I_G ratio of earlier published similar materials.

S.N.	Sample Name	Graphitization Temperature	I _D /I _G ratio	References
1.	T-PAN	1000	0.9	1
2.	PAN nanofiber	2100	1.07	2
3.	PAN/CNT	1000	2.5	3
4.	HGBPC	700	0.906	4
5.	PAA-1300	1300	1.1	5
6.	5Ni@CNF	900	0.97	6
7.	CF-PIM-1	800	1.16	7
8	CNF-Co10	1000	0.9	8
9.	NHPC800	800	1.078	9

References:

- (1) Ma, T.; Shao, R.; Wang, W.; Liu, S.; Min, C.; Jiang, W.; Li, T.; Xu, Z. Enhanced graphitization and reduced radial heterogeneity of carbon fibers inheriting from irradiated/thermo-chemically stabilized PAN-fibers. *Polymer* **2024**, *308*, 127347. DOI: <https://doi.org/10.1016/j.polymer.2024.127347>.
- (2) Hwang, Y. W.; Shin, T. J.; Seo, J. H.; Kim, M. H.; Lee, W. J.; Ruoff, R. S.; Seong, W. K.; Lee, S. H. Effect of Sample Geometry on Graphitization of Polyacrylonitrile. *Small* *n/a* (n/a), 2400301. DOI: <https://doi.org/10.1002/sml.202400301>.
- (3) Ali, A. B.; Slawig, D.; Schlosser, A.; Koch, J.; Bigall, N. C.; Renz, F.; Tegenkamp, C.; Sindelar, R. Polyacrylonitrile (PAN) based electrospun carbon nanofibers (ECNFs): Probing the synergistic effects of creep assisted stabilization and CNTs addition on graphitization and low dimensional electrical transport. *Carbon* **2021**, *172*, 283-295. DOI: <https://doi.org/10.1016/j.carbon.2020.10.033>.
- (4) Tan, Y.; Xu, Z.; He, L.; Li, H. Three-dimensional high graphitic porous biomass carbon from dandelion flower activated by K₂FeO₄ for supercapacitor electrode.

Journal of Energy Storage **2022**, *52*, 104889. DOI: <https://doi.org/10.1016/j.est.2022.104889>.

(5) Feng, J.; Hu, P.; Cheng, Y.; Wang, Y.; Qu, N.; Zheng, L.; Xun, L.; Zhang, C.; Zhao, G.; Zhang, X. Polyarylacetylene as a novel graphitizable precursor for fabricating high-density C/C composite via ultra-high pressure impregnation and carbonization.

Journal of Materials Science & Technology **2024**, *182*, 198-209. DOI: <https://doi.org/10.1016/j.jmst.2023.09.044>.

(6) Chanthee, S.; Asavatesanupap, C.; Sertphon, D.; Nakkhong, T.; Subjaleearndee, N.; Santikunaporn, M. Electrospinning with Natural Rubber and Ni Doping for Carbon Dioxide Adsorption and Supercapacitor Applications. *Engineered Science* **2024**, *27*, 975. DOI: 10.30919/es975.

(7) Patil, B.; Satilmis, B.; Uyar, T. Metal-free N-doped ultrafine carbon fibers from electrospun Polymers of Intrinsic Microporosity (PIM-1) based fibers for oxygen reduction reaction. *Journal of Power Sources* **2020**, *451*, 227799. DOI: <https://doi.org/10.1016/j.jpowsour.2020.227799>.

(8) Barhoum, A.; Favre, T.; Sayegh, S.; Tanos, F.; Coy, E.; Iatsunskyi, I.; Razzouk, A.; Cretin, M.; Bechelany, M. 3D Self-Supported Nitrogen-Doped Carbon Nanofiber Electrodes Incorporated Co/CoO_x Nanoparticles: Application to Dyes Degradation by Electro-Fenton-Based Process. *Nanomaterials* **2021**, *11* (10), 2686.

(9) Xiao, J.; Zhan, B.; He, M.; Qi, X.; Gong, X.; Yang, J.-L.; Qu, Y.; Ding, J.; Zhong, W.; Gu, J. Interfacial Polarization Loss Improvement Induced by the Hollow Engineering

of Necklace-like PAN/Carbon Nanofibers for Boosted Microwave Absorption.

Advanced Functional Materials n/a (n/a), 2316722. DOI:

<https://doi.org/10.1002/adfm.202316722>.